Reverse mutational scanning of spike BA.2.86 identifies epitopes contributing to immune escape from polyclonal sera

Najat Bdeir[1], Tatjana Lüddecke[1], Henrike Maaß[1], Stefan Schmelz[2], Ulfert Rand[3], Henning Jacobsen[1], Kristin Metzdorf[1], Upasana Kulkarni[1], Anne Cossmann[4], Metodi V. Stankov[4], Markus Hoffmann[5,6], Stefan Pöhlmann[5,6], Wulf Blankenfeldt[2,7], Alexandra Dopfer-Jablonka[4,8], Georg M.N. Behrens[4,8,9#], Luka Čičin-Šain*[1,8,9#]

[1] Department of Viral Immunology, Helmholtz Centre for Infection Research, Braunschweig, Germany

[2] Department Structure and Function of Proteins, Helmholtz Centre for Infection Research Braunschweig, Germany

[3]DSMZ- German Collection of Microorganisms and Cell Cultures, Braunschweig, Germany

[4] Department of Rheumatology and Immunology, Hannover Medical School, Hannover, Germany

[5] Infection Biology Unit, German Primate Center – Leibniz Institute for Primate Research, Göttingen, Germany

[6] Faculty of Biology and Psychology, University Göttingen, Göttingen, Germany

[7] Institute for Biochemistry, Biotechnology and Bioinformatics, Technische Universität Braunschweig, Braunschweig, Germany

[8] German Center for Infection Research, partner site Hannover-Braunschweig, Hannover, Germany

[9] Centre for Individualized Infection Medicine, a joint venture of HZI and Hannover Medical School, Hannover, Germany

# These authors contributed equally *For correspondence: Luka Čičin-Šain: Luka.Cicin-Sain@helmholtz-hzi.de

ABSTRACT

The recently detected Omicron BA.2.86 lineage contains more than 30 amino acid mutations relative to BA.2. BA.2.86 and its JN.1 derivative evade neutralization by serum antibodies of fully vaccinated individuals. In this study, we elucidate epitopes driving the immune escape of BA.2.86 and JN.1 via pseudovirus neutralization. Thus, we have generated 33 BA.2.86 mutants, each reverting a single mutation back to BA.2. We use this library in an approach that we call reverse mutational scanning to define distinct neutralization titers against each epitope. Mutations within the receptor binding domain at K356T, V483Δ, and to a lesser extent N460K, A484K, and F486P enhance immune escape. Interestingly, 16insMPLF within the spike N-terminal domain and P621S within S1/S2 also significantly contribute to antibody escape of BA.2.86. Upon XBB.1.5 booster vaccination, neutralization titers against JN.1 and BA.2.86 improve considerably, and a residual immune escape is driven by 16insMPLF, N460K, E554K, and to a lesser extent P621S, and A484K.

EDITOR'S SUMMARY

SARS COV2 Omicron lineage BA.2.86 has over 30 mutations compared to the parental BA.2 lineage. Here Bdeir and colleagues apply reverse mutational scanning to determine which among these mutations present in Omicron BA.2.86 are epitopes linked to immune escape from antibody recognition.

INTRODUCTION

The emergence of new SARS-CoV-2 virus lineages continues to be a critical aspect of the ongoing epidemic viral spread. Among these lineages, BA.2.86, also known as Pirola, has garnered recent attention owing to its significant antigenic shift away from the prevailing XBB sub-lineage [2,3]. The earliest detection of BA.2.86 was in late July 2023 in Denmark [4-6]. By mid-august, it had been detected within several countries and WHO had classified it as a variant of interest [5-7]. An outbreak of BA.2.86 recorded in the United Kingdom with a high attack rate (86.6%) within an elderly care home demonstrated the transmissibility of this lineage [8]. At present, the extent of disease severity exerted by BA.2.86 is unclear, but its derivative sub-variant JN.1 is on track to become the globally dominant SARS-CoV-2 lineage.

The viral spike (S) protein mediates SARS-CoV-2 host cell entry through a multistep process. The initial step involves binding of the S protein to angiotensin converting enzyme-2 receptors (ACE2). This engagement is followed by S protein cleavage by host cell proteases, enabling the S protein to drive fusion of the viral envelope with cellular membranes [9]. The S1 domain of the S protein entails an N-terminal domain (NTD) with somewhat unclear functions, and the receptor-binding domain (RBD), which directly binds to ACE2 and is the major target for neutralizing antibodies [9-11]. The transmembrane S2 domain drives viral fusion with the host cell membrane, which facilitates the release of viral genetic material into the cytoplasm, and therefore plays an important role in infection. BA.2.86 harbors more than 30 mutations relative to BA.2, encompassing 13 mutations in NTD, 14 in the RBD, and 7 within the pre S1/S2 and S2 domain [12]. Furthermore, several BA.2.86 descendants have been identified, including BA.2.86.1 (defining mutation ORF1a:K1973R), JN.1 (L455S), JN.2 (ORF1a:Y621C), JN.3 (ORF1a:T2087I), and BA.2.86.2 (ORF7a:E22D)[3].

The alarming number of BA.2.86 spike mutations has prompted several efforts to characterize the antibody immune escape potential of this lineage. Recent studies demonstrate

reduced pseudo-virus neutralization of BA.2.86 and JN.1 in comparison to BA.2 and B.1 strains and that vaccination with the monovalent BNT162b2 XBB.1.5 adapted vaccine significantly enhances neutralization of BA.2.86 pseudo virus by serum antibodies [13-15]. However, the contribution of single mutations to the immune escape of BA.2.86 remains unclear. Mutational scanning approaches, where libraries of viruses with single amino acid mutations in the spike protein are compared to the wild-type virus are powerful tools for the identification of epitopes recognized by monoclonal antibodies [16-18], but polyclonal serum antibodies recognize numerous epitopes simultaneously and redundantly. Therefore, mutating one out of 33 epitopes on an ancestral background may only marginally decrease the serum neutralizing activity if some among the remaining 32 epitopes are recognized by independent antibody clones. To overcome this limitation, we cloned a library of 33 reversion mutants on the BA.2.86 background, each harboring a single mutation reverting the position back to the amino acid in BA.2. This approach allowed us to observe a robust increase in neutralizing activity whenever an immunologically relevant epitope was reintroduced in the spike. We tested this library of BA.2.86 mutants against serum samples collected from a cohort of 30 healthcare workers, before and after vaccination with the BNT162b2 XBB.1.5 adapted vaccine. Our data showed that mutations ins16MPLF, K356T, N460K, V483Δ, A484K, F486P and S621P distributed across NTD, RBD, and S1/S2 domains, contribute to the immune escape of BA.2.86. Additionally, we show that vaccination with the BNT162b2 XBB.1.5 adapted vaccine increases substantially the neutralization titers against both BA.2.86 and the more recent BA.2.86.1.1 (JN.1) descendant, and that the immune escape of JN.1 is more pronounced than that of BA.2.86 before and after XBB.1.5 booster vaccination. Moreover, we demonstrate that the deletion of the MPLF insertion at position 16, reversions of N460K and K554E, and to lesser extent the reinsertion of the tyrosine residue at position 144, as well as S621P and K484A improve neutralization of BA.2.86 upon the XBB.1.5 booster shot.

RESULTS

BA.2.86 spike protein harbors a substantial amount of mutations within all domains

The analysis of the BA.2.86 spike sequence (specifically: hCoV-19/Denmark/DCGC-647694/2023, EPI_ISL_18114953) revealed 33 mutations relative to BA.2 spike (Figure 1). These include 13 mutations within the NTD, 14 mutations in the RBD, and 6 mutations within the S2 and pre S1/S2 domain. Of these mutations, there are five deletions (H69Δ, V70Δ, Y144Δ, N211Δ, and V483Δ) and one insertion after V16 (V16insMPLF). Among mutations that have been previously identified in other variants of interest are R21T (B.1.617), H69Δ/V70Δ (B.1.1.7/Alpha), Y144Δ (XBB.1.5; EG.5.1; BA.1), R158G (B.1.617.2/Delta), E484K (B.1.351/Beta; P.1/Gamma) and P681R (B.1.617.2/Delta). Additionally, BA.2.86 harbors several mutations, which were rarely reported (V445H, N450D, N481K, V483Δ; and E554K) [19-21]. Among these mutations ins16MPLF, ΔY144, F157S, R158G, H245N, A264D are located within the NTD antigenic supersite and may contribute to immune escape [22]. Additionally, several mutations within the RBD of BA.2.86 have been associated with antibody resistance including K356T, A484K, and N450D [10,23,24], while several other mutations R493Q, F486P, N460K, and V483Δ may alter ACE2 interactions [25,26]. Hence, BA.2.86 contains a plethora of mutations within the spike protein, which may alter key properties of this virus in receptor binding and neutralizing antibody escape. To visualize the position of mutations in the spike protein of BA.2.86 with respect to BA.2, we used AlphaFold2/AlphaFold-Multimer [27,28] to construct a structural model of the spike trimer of BA.2.86. The model, which was obtained in a closed state with respect to the conformation of the RBD, shows that mutations with respect to BA.2 are spread over the distal part of the protein but otherwise do not cluster at specific positions (Fig. 1B-C).

126

127 **BA.2.86 and JN.1 efficiently escape antibody neutralization**

128 To assess the immune escape of the BA.2.86 and BA.2.86.1.1 (JN.1) lineages, we employed
129 pseudo-virus particles (pp) in neutralization assays. For comparison, we also included particles
130 harboring the spike protein of XBB.1.5 ($XBB.1.5_{pp}$), Wuhan-Hu-01 (WT_{pp}), BA.1 ($BA.1_{pp}$),
131 and BA.2 ($BA.2_{pp}$) (Figure 2A-B). We found that plasma obtained from a cohort of at least
132 double boostered individuals neutralized $BA.1_{pp}$ and $BA.2_{pp}$ 3-fold reduced efficiency as
133 compared to the index $WT_{pp,}$. However, the inhibition of $BA.2.86_{pp}$ and $XBB.1.5_{pp}$ was 57-
134 and 48-fold reduced, respectively (Figure 2A). Antibody escape of $JN.1_{pp}$ was even more
135 pronounced, with a ~141-fold reduction relative to WT_{pp} (Figure 2A). Plasma acquired post
136 vaccination with the XBB.1.5-adapted mRNA vaccine neutralized $XBB.1.5_{pp}$ and $BA.2.86_{pp}$,
137 with almost comparable efficiency, whereby the mean neutralization titer was 9-fold and 11-
138 fold lower than WT_{pp}, respectively, while $JN.1_{pp}$ was 27 fold lower (Figure 2B). Collectively,
139 $BA.2.86_{pp}$ and $JN.1_{pp}$ escaped neutralization by antibodies induced upon primary vaccination
140 series and boosters with immunogens predating XBB lineages, whereby this escape was more
141 pronounced in JN.1. However, a vaccination with the XBB.1.5 adapted vaccine boosted the
142 neutralizing titers against both variants and reduced the gap in neutralization efficiency
143 between them and Omicron BA.2. The neutralization efficiency of $JN.1_{pp}$ was ~2.4 fold
144 reduced relative to $BA.2.86_{pp}$, before and after XBB.1.5 booster vaccination.

145 **Mutations ins16MPLF, K356T, N460K, V483Δ, A484K, F486P, and P621S contribute to**
146 **BA.2.86 neutralizing antibody escape.**

147 To investigate the effect of individual mutations within BA.2.86 on post-vaccination
148 neutralizing antibody escape, we cloned a comprehensive library of 33 individual BA.2.86
149 mutants. Each of them contains a single reversion relative to the amino acid sequence of BA.2,

while retaining the rest of the sequence as in BA.2.86. Geometric means of pseudo-virus neutralization titers (PVNT50) against $BA.2.86_{pp}$ were ~18-fold lower than against $BA.2_{pp}$ prior to vaccination with the XBB.1.5 vaccine (Figure 3A). Hence, we tested which mutations decreased the gap between neutralization of $BA.2_{pp}$ and $BA.2.86_{pp}$. Our data showed that among the $BA.2.86_{pp}$ mutants with single mutations within the NTD, only the insMPLF16Δ_{pp} reduced the gap to $BA.2_{pp}$ to a mere 4-fold reduction (Figure 3A). The remaining NTD_{pp} single mutants did not significantly contribute to neutralizing antibody escape, because their neutralization titers were comparable to that of $BA.2.86_{pp}$ (Figure 3B). Moreover, we have shown in Zhang et al, that insMPLF16Δ leads to a reduction of infectivity in VeroE6 cells [29] . Hence, this unique NTD mutation is involved in both immune evasion from sera antibodies and infectivity. While the N-terminus of BA.2.86 spike protein is modelled with lesser confidence than the core of the structure (Figure S1A-C), it is interesting that the N-terminal 16MPLF insertion is predicted to interact with a crevice in the N-terminal domain (NTD; Figure S1B-C). This is reminiscent of SARS-CoV spike protein [30], albeit here, the N-terminus is yet more extended and anchored via a disulfide bridge to the core of the NTD (Figure S1D). Structural modelling from Colson et. al.[31] also suggest that insMPLF16 masks a V-shaped electronegative zone within the NTD which might allow an advantage to stabilize the virus on target cells. It may also induce long range conformational rearrangements affecting the RBD and potentially RBD-ACE2 interactions.

The neutralization capacity of serum samples against epitopes in the RBD of $BA.2.86_{pp}$ was significantly affected prior to the XBB.1.5 booster by the mutation K356T and ΔV483, which had a 6 or 7 fold reduction in neutralization titer relative to BA.2, respectively (Figure 4A and 4B). Additionally, our results showed that $K460N_{pp}$, , $K484A_{pp}$, and $P486F_{pp}$ had a 6-, 7-, and 8-fold reduced neutralization efficiency, respectively, relative to $BA.2_{pp,}$ and thus much less than the 18-fold reduction observed in $BA.2.86_{pp}$. While the latter results did not raise to

175 statistical significance over BA.2.86$_{pp}$ (Fig. 4B), they indicated an improved neutralization in
176 the presence of these parental epitopes. In contrast, the remaining mutations within the RBD
177 of BA.2.86 did not enhance serum neutralization capacity.

178 In addition to the aforementioned RBD and NTD BA.2.86 mutants, we explored the
179 contribution of mutations within the S1/S2 and S2 regions to antibody evasion. We report a
180 significant increase in neutralization efficiency for BA.2.86 S621P$_{pp}$, whereby neutralization
181 efficiency of BA.2.86 S621P$_{pp.}$ was 4-fold lower than that of BA.2$_{pp}$ and hence, significantly
182 higher than for BA.2.86$_{pp}$ (Figure 5A and 5B) In contrast, BA.2.86 K554E$_{pp}$, V570A$_{pp}$,
183 R681H$_{pp}$, F939S$_{pp}$, L1143P$_{pp}$ all showed comparable neutralization sensitivity as compared to
184 BA.2.86$_{pp}$ (Figure 5A, and 5B).

185 Interestingly, the impact of BA.2.86 mutations on neutralization escape following vaccination
186 with the adapted XBB.1.5 immunogen revealed that the mutants insMPLF16Δ$_{pp}$, K554E$_{pp}$, and
187 K460N$_{pp}$ significantly recovered the neutralization efficiency of plasma samples above
188 BA.2.86$_{pp}$ and to levels comparable to that of BA.2 neutralization (Figure 6). An increase in
189 neutralization efficiency after XBB.1.5 booster vaccination was observed for BA.2.86 mutants
190 S621P$_{pp}$, ins144Y$_{pp}$ and K484A$_{pp}$, but it did not raise to statistical significance, (Figure 6).
191 Further information on the post vaccination neutralization titers for each mutant pseudovirus
192 is provided in supplementary data (Figure S2 and Supplementary data 2). Since neutralization
193 efficiency of JN.1$_{pp}$ was merely 2.4 fold reduced relative to BA.2.86$_{pp}$ after the XBB.1.5
194 booster vaccination, our data may argue that these positions may be relevant for the residual
195 immune escape of JN.1 upon the XBB.1.5 booster as well.

196 We previously reported that pseudovirus infectivity of Vero cells was significantly perturbed
197 in Δins16MPLF, K403R, D450N, Q493R, and S621P [29]. Since a reduction in infectivity may
198 reflect an increase of dysfunctional virions in a stock, which would act as sponges for

neutralizing antibodies and compete with infectious particles [1], we performed a digital droplet PCR (ddPCR) of VSV-N stocks, thus defining the genome copy number relative to infectious virus titers. For all tested mutants, these numbers were clustering between those of BA.2 and BA2.86 (Supplementary information, Fig. S3). Therefore, our results all but exclude the possibility that the neutralization titers were affected by the infectivity of the individual epitope mutants.

Discussion

This work provides to our knowledge the first example of a reverse mutational scanning strategy for the identification of epitopes that contribute to immune escape from vaccine-induced immunity. Strategies based on mutational scanning of the SARS-CoV-2 spike are not new. Others and we have shown that such approaches can be used to generate libraries containing individual mutations present in the Omicron, but not in the ancestral variants, and thus identify epitopes that escape recognition by monoclonal antibodies [17,18] and polyclonal sera [1,16,17]. A very comprehensive mutational scanning based on the XBB.1.5 spike has been recently performed by the Bloom lab to introduce 9000 theoretical mutations on the XBB.1.5 background and thus predict future potential escape mutations [16]. However, forward mutational scanning cannot predict the emergence of lineages with big evolutionary jumps, such as the Omicron BA.1 and BA.2.86 variants, where more than 30 mutations were observed simultaneously, with no intermittent stages that are known. Moreover, such approaches are not ideal for the analysis of neutralizing potential of polyclonal sera, where redundant epitope recognition may result in virus neutralization even if immunologically relevant epitopes are mutated. Indeed, a forward mutational scanning approach that we have employed in a previous study to assess Omicron epitope mutations on a Wuhan background showed only modest (<twofold) reductions in neutralization titers [1]. By reverse mutational scanning, we provide here a loss-of-function genetic approach, allowing the identification of up to fourfold

differences in titers. Thus, we were able to identify escape epitopes in polyclonal responses to antigens with many simultaneous mutations, defining the collection of epitopes that contribute to immune escape from vaccine-induced immunity by BA.2.86 and its derivative JN.1 lineage. This approach may also be rapidly deployed for subsequent lineages with big evolutionary jumps that may emerge in the future.

The emergence of BA.2.86 harboring more than 30 mutations relative to BA.2 was reminiscent of the Omicron appearance in 2021 and raised concerns regarding its antibody escape potential [13,14,32]. A number of these mutations (K356, V445, G446, N450, L452, and P621) were also observed in omicron sub-lineages within immunocompromised patients. This may indicate that reduced immune functions within some individuals may be a source of highly mutated SARS-CoV2 lineages [33,34]. BA.2.86 has also evolved several descendants including JN.1 which harbors three mutations in non S-proteins and a hallmark S455L mutation in the spike protein [3]. In plasma from a cohort that was at least double boostered, we observed that the S455L mutation reduces the neutralization efficiency relative to BA.2.86 by a factor of ~2.5, but that the XBB.1.5 adapted vaccine booster increases neutralization efficiency against both lineages roughly ~12 to 13 fold, in line with data reported in Stankov et al. [35] and Wang et al. [14]. Moreover, neutralization of $BA.2.86_{pp}$ and $JN.1_{pp}$ were merely 1.2-fold and 3 fold lower than the neutralization of Omicron XBB.1.5 respectively. Nevertheless, their neutralization titers remain 6- and 16 fold lower than that of BA.2 following vaccination respectively.

Several mutations within BA.2.86 significantly increased the neutralizing antibody escape prior to vaccination with the adapted XBB.1.5 vaccine. We found that the NTD mutation ins16MPLF significantly affected neutralization sensitivity, and its reversion resulted in a 4-fold increase in neutralization titers relative to BA.2.86. While this region of the NTD is disordered in published structures of the SARS-CoV-2 spike protein, indicating high intrinsic flexibility, the MPLF insertion is somewhat reminiscent of the SARS-CoV spike protein, where

the N-terminus is yet more extended and anchored via a disulfide bridge to the core of the NTD (Fig. S1D). It should be noted that several NTD-binding neutralizing antibodies have been identified in the past [36,37], indicating that mutations in this domain may indeed interfere with the immune system's capacity to recognize the virus. Even more interestingly, we show that the deletion of the MPLF insertion at position 16 significantly increases neutralization efficiency after the adapted XBB.1.5 vaccination to BA.2 comparable levels. This mutation is located within the NTD antigenic supersite, which is a key target for NTD specific neutralizing antibodies [22]. Moreover, in silico structural modeling of BA.2.86 performed by Colson et al. indicates that the MPLF insertion may mask a V-shaped electronegative zone within the NTD, which is an unprecedented phenotype in SARS-CoV-2. This zone may stabilize the virus onto target cells and may induce some long-range conformational changes which affect the RBD with potential consequences on RBD-ACE2 interactions [31]. However, our independent in silico analysis of this region of the NTD structure argues that the changes at the N-terminal tip cannot be predicted with a high degree of confidence. Therefore, the actual effects of this mutation on the NTD structure may only be confirmed by empirical analysis in cryoelectron microscopy or similar approaches.

We also found that the mutation K356T within the RBD plays a contributing role to BA.2.86 escape of neutralization by polyclonal sera, whereby it lead to a six-fold reduction in neutralization efficiency relative to $BA.2_{pp}$, in comparison the 18 fold reduction in the case of $BA.2.86_{pp}$. This reduction in neutralization efficiency might be attributed to the steric hindrance caused by the introduction of an additional glycosylation site [38]. Similarly, we show that mutations N460K, V483Δ, A484K, and F486P within the RBD may enhance neutralizing antibody escape. This is in line with reports from Wang et al, which show that mutation N460K and F486P shared in XBB.1.5 and EG.5.1 cause resistance to class 1 and 2 monoclonal antibodies (mAb) [39]. Structural modelling has shown that the mutation N460K, which was first

identified in BA.2.75, disrupts a hydrogen bond formed between the RBD and a class 1 mAb (VH3-53) [40] and a study by Wang et al. demonstrated that the mutation A484K within BA.2.86 reduced the neutralizing activity of a subset of class 3 mAbs [14]. The mutation V483Δ has seldom been reported in circulating strains. Full spike mutational scanning of BA.2.86 postulated that V483Δ may contribute to antibody escape but experimental evidence for this has been lacking [16]. We also show that the mutation P621S in the S1/S2 domain of BA.2.86 contributed to significant neutralization escape and this phenotype, to our knowledge has not been demonstrated previously. In sum, we have identified several mutations that have significantly contributed to immune escape in our cohort. However, we cannot exclude that additional mutations may result in immune escape in individuals whose repertoire differs from our cohort of double boostered individuals. This requires additional studies in cohorts of elderly people or those with immune deficiencies. In parallel to our present study, we have conducted a more thorough investigation to explore the effects of BA.2.86 specific mutations on infectivity and cell entry, including ACE-2 binding and protease usage [29]. We observed that lung cell entry of BA.2.86 is ACE2 dependent and is markedly more efficient than that driven by the S proteins of other omicron sublineages. To obtain insights into which amino acids are critical to this phenotype, we explored the infectivity of every pseudoviral mutant on Vero and Calu-3 lung cells. This revealed that BA.2.86 specific mutations at NTD residue L50 and RBD residue T356 specifically promote lung cell entry and bear no relevance for Vero cells' entry. Several mutations affected cell entry into Vero cells, up to a sevenfold reduction in infectivity.

We have shown previously that mutant viruses with a hundred fold impaired infectiveness display a quantifiable reduction in neutralization serum titers due to the preponderance of non-infectious virus particles in the virus stock that act as antibody sponges in the neutralization assay [1]. Thus, we checked if the pseudovirus stocks showing significant differences in the cell entry assay into Vero cells [29] or in the neutralization assay had more non-

infectious particles (Supplementary information, Fig. S3), but we observed no substantial differences relative to the parental BA.2 or the index BA.2.86 strain. Hence, effects of individual mutations on Vero cell infectivity was unlikely to have affected our neutralization results.

It is also important to acknowledge some pertinent limitations relating to our study. We have utilized the well-established pseudo-virus system to assess the contribution of single mutations to the antibody escape potential of BA.2.86. While formal verification would require the use of authentic SARS-CoV-2 with spike mutations introduced by reverse genetics, neutralization titers in pseudo-viral and authentic virus setups have been shown to be comparable due to the immunodominance of spike over other structural elements [41-43]. An additional limitation in our study is the lack of information regarding hybrid immunity within our cohort, whereby some participants may have experienced a prior unrecorded infection with XBB sublineages, which may have elicited a humoral immune response similar to vaccination. However, only 4 individuals have a recorded infection in 2023, when the XBB.1.5 lineage was present at high levels.

In sum, BA.2.86 and its JN.1 descendent efficiently escape neutralization by polyclonal serum antibodies of at least double boostered individuals, and our data argue that this is due to mutations at positions N460K, V483Δ, A484K, F486P, K356T, P621S, and ins16MPLF. We also observed that the S455L mutation provides a 2-fold decrease in neutralization titers over BA.2.86. However, neutralization titers of JN.1 and BA.2.86 were appreciably improved by the XBB.1.5 vaccine booster, whereby JN.1 has a mere 2.5 reduction relative to BA.2.86 . This may argue that residual immune escape of both lineages may rely on the shared epitopes at positions ins16MPLF, E554K, N460K, and to lesser extent A484K and Y144Δ.

Methods

Cell lines

All cell lines were maintained at 37 °C and 5% CO_2 in a humified environment. 293T (Human, kidney) and VeroE6 (African green monkey, kidney) cells were cultured in Dulbecco's Modified Eagle Medium (DMEM, ThermoFisher Scientific) supplemented with 5% fetal bovine serum (FBS, ThermoFisher Scientific) and 100 U/ml penicillin and 0.1 mg/ml Streptomycin (PAN-Biotec). Both cell lines were used to a maximum passage of 30. For seeding and sub-cultivation, cells were washed with phosphate buffered saline (PBS, PAN-Biotec) and then incubated with trypsin/EDTA (PAN-Biotec) until cell detachment. Cell lines were routinely tested for mycoplasma. The origin and catalogue numbers of cells are shown in table 1, Supplementary data 3. Transfection of 293T cells for the production of pseudoviruses was carried out by calcium phosphate transfection.

Plasmids

The plasmid pCG1_SARS-2-Sdel18 (Codon-optimized) encoding the spike protein of the Wuhan-Hu-1 SARS-CoV-2 has been previously reported [9]. The pCG1_SARS-2-Sdel18 BA.1 and BA.2 expression plasmids are previously reported [1] and based on isolate hCoV-19/Botswana/R40B58_BHP_3321001245/2021 (GISAID Accession ID: EPI_ISL_6640919) and isolate hCoV-19/England/PHEC-4G0AFZF7/2021 (GISAID Accession ID: EPI_ISL_8738174) respectively. The pCG1_SARS-2-Sdel18 XBB expression plasmid was generated by Gibson assembly based on the expression vector for the spike of Omicron BA.2 and site directed mutagenesis was done to generate XBB.1.5. Expression plasmids pCAGGS-DsRed and pCG1-SARS-2-SDel18 BA.2.86 (based on the isolate hCoV-19/Denmark/DCGC-647694/2023, EPI_ISL_18114953) were kindly provided by the Laboratory of Stefan Pöhlmann (Table 3, Supplementary data 3). Site directed mutagenesis (Q5® High-Fidelity 2X Master Mix, New England BioLabs) was utilized for the generation of the SARS-CoV-2 spike

BA.2.86 expression plasmid library containing single point mutations back to BA.2 spike. Transformation was carried out using NEB® 10-beta Competent E. coli from New England BioLabs (catalogue: C3019H). Primers are listed in Table 2, Supplementary data 3.

Production and titration of Pseudo-viruses

Production of pseudo-viruses was performed according to published protocol [44]. In brief, 293T cells were seeded in 6 well plates at a confluency of 70%. The next day, cells were transfected with expression plasmids for pCG1-SARS-2-SΔ18 WT, pCG1-SARS-2-SΔ18 BA2.86, pCG1-SARS-2-SΔ18 BA2, pCG1-SARS-2-SΔ18 BA2.86 XBB or pCG1-SARS-2-SΔ18 BA2.86 single point mutants. At 24 hours post transfection, cells were incubated for 1 hour with a replication deficient VSV (VSV*ΔG) expressing enhanced green fluorescent protein (eGFP) and firefly luciferase at an MOI of 3. VSV*ΔG was kindly provided by the lab of Gert Zimmer. Subsequently, cells were washed with phosphate buffered saline (PBS) and incubated with anti-VSV-G antibody (mouse hybridoma supernatant from CRL-2700; ATCC) in order to neutralize residual input virus. At 12 hours post infection, supernatants were harvested and cleared from cell debris by centrifugation and stored at -80C for later use. For titration, aliquots of the pseudo-virus were serially diluted threefold in duplicates, starting with a 1:10 dilution in a 96-well plate, totaling eleven dilutions. The last column served as a control with cells but no pseudo-virus. Confluent VeroE6 cells in the 96-well format were infected with the diluted virus, then incubated for 24 hours at 37°C with 5% CO2. GFP+ infected cells were counted using the IncuCyte S3 (Sartorius), which performed whole-well scans (4x) in phase contrast and green fluorescence (300ms exposure). The IncuCyte GUI software (versions 2019B Rev1 and 2021B) was used for counting of fluorescent foci and counts were exported to Excel 2016. The average number of infected cells was calculated for three different pseudo-virus dilutions, and this number was multiplied by the

dilution factor to determine the focus forming units (ffu) per ml. The pseudo-virus titer was calculated as the mean ffu/ml from the three pseudo-virus dilutions.

Neutralization assay

Neutralization assays were based on a previously published protocol [1]. In brief, all plasma samples utilized in this study were heat inactivated at 56 °C for 30 minutes, 10 fold diluted in DMEM [1% Penicillin-Streptomycin, 1% L-Glu, 5% FBS], and stored at 4 °C for further use. Pseudo-viral particles (600pfu/well±30%) were incubated for one hour in a 96 well microtiter plate with two-fold diluted serum samples in DMEM [1% Penicillin-Streptomycin, 1% L-Glu, 5% FBS] ranging from 1:100 to 1:51200. Pseudo-virus particles were incubated in the absence of plasma as controls indicating 0% inhibition. After incubation, the serum/virus samples were transferred onto a confluent VeroE6 96 well plate. After a 24-hour incubation, plates were fixed with 4% paraformaldehyde (PFA) and stored at 4 °C until readout. GFP+ infected cells were counted using an IncuCyte S3 (Sartorius) performing whole-well scans (4x) in phase contrast and green fluorescence settings (300ms exposure). Automated segmentation and counting of fluorescent foci defined as green fluorescent protein GFP+-single cells was performed using the IncuCyte GUI software (versions 2019B Rev1 and 2021B). Pseudo-virus neutralization titer 50 (PVNT50) values were determined by a non-linear regression model. The lower limit of confidence (LLOC) was set at a PVNT50 of 50. Non-responders were defined as individuals with PVNT50<60 (dashed line). All PVNT50<10 are set at 10 for visualization purposes. Due to technical limitations (the limited volume of plasma samples and the technical challenges associated with assaying 30 samples against ~40 different pseudoviruses in duplicates), every pseudovirus was tested on at least 20 individual, randomly chosen plasma samples. These were arranged so that over 80% of the plasma originated from the same set of patients. This approach

aimed to minimize variability due to differing inherent potencies among plasma samples. All data are presented as numerical titers for each study participant in the supplementary data 2.

Ethics committee Approval

The collection of all plasma samples was approved by the research ethics committee of the Institutional Review Board of Hannover Medical School (8973_BO_K_2020). All donors provided written consent for plasma donation and use research purposes, consent for publishing identifiers such as sex and age was also acquired.

Plasma Samples

The number of participants within this analysis is n=30. Median age is 45 years (interquartile range (IQR) 33 to 56). Male to female ratio is 1:2. Among these participants, 30% were vaccinated with three vaccine doses, 60% were vaccinated with four vaccine doses, and 10% were vaccinated with more than four doses. Ten participants (33.3%) were vaccinated with the bivalent WT/BA.4/5 vaccine. The median time in months since last recorded SARS-CoV-2 infection for the patients with known infections is 15 (IQR 13 to 18). The median number of months since the last known vaccination dates within our cohort is 13,5 months (IQR 11 to 22). All participants are part of the COVID-19 contact study, to monitor anti-SARS-CoV-2 immune responses in healthcare workers at Hannover Medical School (MHH). All participants donated blood directly prior to vaccination with 30µg of the updated BNT162b2 Omicron XBB.1.5 vaccine (Raxtozinameran, BioNTech, Mainz, Germany) in September 2023 and were followed-up for another blood collection 15-16 days post vaccination [35]. Plasma was separated from collected blood and stored at -80 °C for long term storage and 4°C for immediate use. Detailed information is provided in Supplementary data 1.

425 **Viral genome copy number**

426 To quantify the VSV genome copy numbers in samples, digital droplet PCR (ddPCR) was
427 performed on the VSV-N gene. Supernatants containing viral particles were treated with
428 nuclease muncher (Abcam) by incubating with 2 U/ml for >60 min at 37°C before RNA
429 isolation using the QIAamp Viral RNA Mini kit according to the manufacturer's instructions.
430 For ddPCR, a one-step RT-ddPCR kit (Bio-Rad) was used combined with primers and probe
431 detecting the VSV N (qRT VSV-N_F: ATGACAAATGGTTGCCTTTGTATCTACTT,
432 qRT VSV-N R: ACGACCTTCTGGCACAAGAGGT, VSV-NcDNA probe:
433 /56FAM/ACAGAGTGG/ZEN/GCAGAACACAAATGCCT/3IABkFQ/) and, to exclude the
434 presence of non-enveloped RNA in the sample, we used the human ACTB transcript
435 (ACTBcDNA_F: GAGGAGCACCCCGTG, ACTBcDNA_R: GCCTGGATAGCAACGTAC,
436 ACTBcDNA_probe: [HEX]CCCAGATCATGTTTGAGACCTTCAACACC[BHQ1]) PCR
437 was done with a Bio-Rad C1000 Touch thermo cycler, encapsulation and read-out were done
438 with the Bio-Rad QX200 system. Data analysis was carried out with Bio-Rad QX Manager
439 Standard Edition (version 2.1.0.25).

440

441 **Statistical analysis**

442 Statistical analysis was performed using GraphPad Prism 9.0 (GraphPad software).
443 Neutralization titers were plotted as geometric mean titers. A two sided paired non-parametric
444 Friedman test was performed for non-normally distributed data. P values less than 0.05 were
445 considered significant ns, $p > 0.05$; *, $p \leq 0.05$; **, $p \leq 0.01$; ***, $p \leq 0.001$).

446 **Data availability**

447 Values for neutralization titers and information on plasma donors are provided in
448 Supplementary data 1 and 2. Data underlying the generation of the figures are provided as a
449 source data file: Source Data.

References

1 Katzmarzyk, M. *et al.* Systematical assessment of the impact of single spike mutations of SARS-CoV-2 Omicron sub-variants on the neutralization capacity of post-vaccination sera. *Front Immunol* **14**, 1288794, doi:10.3389/fimmu.2023.1288794 (2023).

2 Callaway, E. Why a highly mutated coronavirus variant has scientists on alert. *Nature* **620**, 934, doi:10.1038/d41586-023-02656-9 (2023).

3 Focosi, D., Spezia, P. G. & Maggi, F. SARS-CoV-2 BA.2.86 ("Pirola"): Is it Pi or Just Another Omicron Sublineage? *Vaccines (Basel)* **11**, doi:10.3390/vaccines11111634 (2023).

4 Harris, E. CDC Assesses Risk From BA.2.86, Highly Mutated COVID-19 Variant. *Jama* **330**, 1029, doi:10.1001/jama.2023.16105 (2023).

5 Rasmussen, M. *et al.* First cases of SARS-CoV-2 BA.2.86 in Denmark, 2023. *Euro Surveill* **28**, doi:10.2807/1560-7917.Es.2023.28.36.2300460 (2023).

6 Wannigama, D. L. *et al.* Tracing the new SARS-CoV-2 variant BA.2.86 in the community through wastewater surveillance in Bangkok, Thailand. *Lancet Infect Dis* **23**, e464-e466, doi:10.1016/s1473-3099(23)00620-5 (2023).

7 Lambrou, A. S. *et al.* Early Detection and Surveillance of the SARS-CoV-2 Variant BA.2.86 - Worldwide, July-October 2023. *MMWR Morb Mortal Wkly Rep* **72**, 1162-1167, doi:10.15585/mmwr.mm7243a2 (2023).

8 Reeve, L. *et al.* High attack rate in a large care home outbreak of SARS-CoV-2 BA.2.86, East of England, August 2023. *Euro Surveill* **28**, doi:10.2807/1560-7917.Es.2023.28.39.2300489 (2023).

9 Hoffmann, M. *et al.* SARS-CoV-2 Cell Entry Depends on ACE2 and TMPRSS2 and Is Blocked by a Clinically Proven Protease Inhibitor. *Cell* **181**, 271-280.e278, doi:10.1016/j.cell.2020.02.052 (2020).

10 Lusvarghi, S. *et al.* Key Substitutions in the Spike Protein of SARS-CoV-2 Variants Can Predict Resistance to Monoclonal Antibodies, but Other Substitutions Can Modify the Effects. *J Virol* **96**, e0111021, doi:10.1128/jvi.01110-21 (2022).

11 Zhou, P. *et al.* A pneumonia outbreak associated with a new coronavirus of probable bat origin. *Nature* **579**, 270-273, doi:10.1038/s41586-020-2012-7 (2020).

12 Yang, S. *et al.* Antigenicity and infectivity characterisation of SARS-CoV-2 BA.2.86. *Lancet Infect Dis* **23**, e457-e459, doi:10.1016/s1473-3099(23)00573-x (2023).

13 Uriu, K. *et al.* Transmissibility, infectivity, and immune evasion of the SARS-CoV-2 BA.2.86 variant. *Lancet Infect Dis* **23**, e460-e461, doi:10.1016/s1473-3099(23)00575-3 (2023).

14 Wang, Q. *et al.* Antigenicity and receptor affinity of SARS-CoV-2 BA.2.86 spike. *Nature*, doi:10.1038/s41586-023-06750-w (2023).

15 Qian, W. *et al.* XBB.1.5 monovalent mRNA vaccine booster elicits robust neutralizing antibodies against emerging SARS-CoV-2 variants. *bioRxiv*, 2023.2011.2026.568730, doi:10.1101/2023.11.26.568730 (2023).

16 Dadonaite, B. *et al.* Full-spike deep mutational scanning helps predict the evolutionary success of SARS-CoV-2 clades. *bioRxiv*, doi:10.1101/2023.11.13.566961 (2023).

17 Pastorio, C. *et al.* Determinants of Spike infectivity, processing, and neutralization in SARS-CoV-2 Omicron subvariants BA.1 and BA.2. *Cell Host Microbe* **30**, 1255-1268.e1255, doi:10.1016/j.chom.2022.07.006 (2022).

18 Abassi, L. *et al.* Evaluation of the Neutralizing Antibody STE90-C11 against SARS-CoV-2 Delta Infection and Its Recognition of Other Variants of Concerns. *Viruses* **15**, doi:10.3390/v15112153 (2023).
19 Miller, J. *et al.* Substantial Neutralization Escape by SARS-CoV-2 Omicron Variants BQ.1.1 and XBB.1. *N Engl J Med* **388**, 662-664, doi:10.1056/NEJMc2214314 (2023).
20 Yue, C. *et al.* ACE2 binding and antibody evasion in enhanced transmissibility of XBB.1.5. *Lancet Infect Dis* **23**, 278-280, doi:10.1016/s1473-3099(23)00010-5 (2023).
21 Wang, Q. *et al.* Antibody evasion by SARS-CoV-2 Omicron subvariants BA.2.12.1, BA.4 and BA.5. *Nature* **608**, 603-608, doi:10.1038/s41586-022-05053-w (2022).
22 McCallum, M. *et al.* N-terminal domain antigenic mapping reveals a site of vulnerability for SARS-CoV-2. *Cell* **184**, 2332-2347.e2316, doi:10.1016/j.cell.2021.03.028 (2021).
23 Vellas, C. *et al.* Resistance mutations in SARS-CoV-2 omicron variant in patients treated with sotrovimab. *Clin Microbiol Infect* **28**, 1297-1299, doi:10.1016/j.cmi.2022.05.002 (2022).
24 Mykytyn, A. Z., Fouchier, R. A. & Haagmans, B. L. Antigenic evolution of SARS coronavirus 2. *Curr Opin Virol* **62**, 101349, doi:10.1016/j.coviro.2023.101349 (2023).
25 Huo, J. *et al.* A delicate balance between antibody evasion and ACE2 affinity for Omicron BA.2.75. *Cell Rep* **42**, 111903, doi:10.1016/j.celrep.2022.111903 (2023).
26 Qu, P. *et al.* Evasion of neutralizing antibody responses by the SARS-CoV-2 BA.2.75 variant. *Cell Host Microbe* **30**, 1518-1526.e1514, doi:10.1016/j.chom.2022.09.015 (2022).
27 Tunyasuvunakool, K. *et al.* Highly accurate protein structure prediction for the human proteome. *Nature* **596**, 590-596, doi:10.1038/s41586-021-03828-1 (2021).
28 Richard, E. *et al.* Protein complex prediction with AlphaFold-Multimer. *bioRxiv*, 2021.2010.2004.463034, doi:10.1101/2021.10.04.463034 (2022).
29 Zhang, L. *et al.* SARS-CoV-2 BA.2.86 enters lung cells and evades neutralizing antibodies with high efficiency. *Cell* **187**, 596-608.e517, doi:10.1016/j.cell.2023.12.025 (2024).
30 Yuan, Y. *et al.* Cryo-EM structures of MERS-CoV and SARS-CoV spike glycoproteins reveal the dynamic receptor binding domains. *Nat Commun* **8**, 15092, doi:10.1038/ncomms15092 (2017).
31 Colson, P. *et al.* Emergence of a second SARS-CoV-2 variant with a tremendous genetic leap from its ancestors. *J Med Virol* **95**, e29124, doi:10.1002/jmv.29124 (2023).
32 Sheward, D. J. *et al.* Sensitivity of the SARS-CoV-2 BA.2.86 variant to prevailing neutralising antibody responses. *Lancet Infect Dis* **23**, e462-e463, doi:10.1016/s1473-3099(23)00588-1 (2023).
33 Berkhout, B. & Herrera-Carrillo, E. SARS-CoV-2 Evolution: On the Sudden Appearance of the Omicron Variant. *J Virol* **96**, e0009022, doi:10.1128/jvi.00090-22 (2022).
34 Raglow, Z. *et al.* SARS-CoV-2 shedding and evolution in immunocompromised hosts during the Omicron period: a multicenter prospective analysis. *medRxiv*, doi:10.1101/2023.08.22.23294416 (2023).
35 Stankov, M. V. *et al.* Humoral and cellular immune responses following BNT162b2 XBB.1.5 vaccination. *Lancet Infect Dis*, doi:10.1016/s1473-3099(23)00690-4 (2023).
36 Chi, X. *et al.* A neutralizing human antibody binds to the N-terminal domain of the Spike protein of SARS-CoV-2. *Science* **369**, 650-655, doi:doi:10.1126/science.abc6952 (2020).

37 Suryadevara, N. *et al.* An antibody targeting the N-terminal domain of SARS-CoV-2 disrupts the spike trimer. *J Clin Invest* **132**, doi:10.1172/jci159062 (2022).
38 Wang, Q. *et al.* Evolving antibody evasion and receptor affinity of the Omicron BA.2.75 sublineage of SARS-CoV-2. *iScience* **26**, 108254, doi:10.1016/j.isci.2023.108254 (2023).
39 Wang, Q. *et al.* Alarming antibody evasion properties of rising SARS-CoV-2 BQ and XBB subvariants. *Cell* **186**, 279-286.e278, doi:10.1016/j.cell.2022.12.018 (2023).
40 Wang, Q. *et al.* Antigenic characterization of the SARS-CoV-2 Omicron subvariant BA.2.75. *Cell Host Microbe* **30**, 1512-1517.e1514, doi:10.1016/j.chom.2022.09.002 (2022).
41 Lester, S. *et al.* Middle East respiratory coronavirus (MERS-CoV) spike (S) protein vesicular stomatitis virus pseudoparticle neutralization assays offer a reliable alternative to the conventional neutralization assay in human seroepidemiological studies. *Access Microbiol* **1**, e000057, doi:10.1099/acmi.0.000057 (2019).
42 Tolah, A. M. K. *et al.* Evaluation of a Pseudovirus Neutralization Assay for SARS-CoV-2 and Correlation with Live Virus-Based Micro Neutralization Assay. *Diagnostics (Basel)* **11**, doi:10.3390/diagnostics11060994 (2021).
43 Quandt, J. *et al.* Omicron BA.1 breakthrough infection drives cross-variant neutralization and memory B cell formation against conserved epitopes. *Sci Immunol* **7**, eabq2427, doi:10.1126/sciimmunol.abq2427 (2022).
44 Berger Rentsch, M. & Zimmer, G. A vesicular stomatitis virus replicon-based bioassay for the rapid and sensitive determination of multi-species type I interferon. *PLoS One* **6**, e25858, doi:10.1371/journal.pone.0025858 (2011).
45 Jumper, J. *et al.* Highly accurate protein structure prediction with AlphaFold. *Nature* **596**, 583-589, doi:10.1038/s41586-021-03819-2 (2021).

ACKNOWLEDGEMENTS:

This research was funded by the Helmholtz Association through Helmholtz Campaign COVIPA (KA1-Co-02) to L.C-S. and EU-Partnering grant MCMVaccine (PIE-008) to L.C-S. and S.P. Funding to L.C-S and S.P. was also provided by the Ministry of Science and Culture of Lower Saxony, through the COFONI Network, flex fund projects 6FF22 and 10FF22. L.C-S also obtained funding from the German Scientific Foundation (DFG) through grants EXC 2155 “RESIST”—Project ID 39087428 and FOR2830, project 5.

G.M.N.B. and A.D.-J. acknowledge funding from Ministry of Science and Culture of Lower Saxony (14-76103-184, COFONI Network, project 4LZF23), G.M.N.B. acknowledges funding by the European Regional Development Fund (ZW7-85151373), and A.D.-J. acknowledge funding by European Social Fund (ZAM5-87006761).

We thank Ayse Barut, Yuliia Polianska, Inge Hollatz-Rangosch and Karina Watzke for expert technical assistance, Natascha Gödecke for support with biosafety compliance and Gert Zimmer (Institute of Virology and Immunology, Mittelhäusern, Switzerland) for providing the VSV pseudo-virus system. We also thank the CoCo Study participants for their support and the entire CoCo study team, especially Annika Heidemann and Luis Manthey, for technical and logistical support.

AUTHOR CONTRIBUTIONS

Conceptualization: LC-S; Methodology: LC-S; NB; Investigation: NB, TL, HM, KM, HJ, SS. UK, UR; Formal analysis: NB, SS, WB, UR, AD-J, GMN, LC-S; Resources: SP, MH, AC,MVS, AD-J, and GMN; Funding acquisition: LC-S; Writing original draft: NB.; Writing review & editing: all authors.

COMPETING INTERESTS

L.C-S. served as an advisor to Sanofi unrelated to this work. G.M.N.B. served as advisor for Moderna unrelated to this work, A.D-J served as an advisor for Pfizer unrelated to this work,

S.P. and M.H. conducted contract research (testing of vaccinee plasma for neutralizing activity against SARS-CoV-2) for Valneva unrelated to this work. S.P. served as advisor for BioNTech, unrelated to this work. H.J. served as advisor on COVID neutralization assays for WHO and CEPI, unrelated to this work. The other authors declare no competing interests.

FIGURES LEGENDS

Figure 1. Overview of BA.2.86 lineage specific spike protein mutations relative to BA.2

(A) Schematic representation of the SARS-CoV-2 spike domains and amino acid changes indicated for BA.2.86, and shared by XBB.1.5, and EG.5.1 compared to the spike of BA.2. Further mutations within XBB.1.5 and EG.5.1 relative to BA.2 are not shown, as only sites mutated within BA.2.86 are represented. N-terminal domain (NTD, blue), receptor binding domain (RBD, green), Subdomains 1 and 2 (SD1 and SD2, orange), S2 subunit (orange). Created in BioRender. Bdeir, N. (2024) BioRender.com/m05k539 and in the references add: Bdeir, N. (2024). Figure 1A. Created in BioRender. BioRender.com/m05k539. (B) Model of the trimeric spike protein of BA.2.86, calculated with AlphaFold2/AlphaFold-Multimer [28,45]. The N-terminal secretion signal (15 residues) and the C-terminal membrane-anchoring sequence (112 residues) were omitted from calculations, leading to 3372 residues in the final model. Domains have been colored according to panel (A), and one of five independently calculated models is shown. Spheres represent the location of mutations with respect to the spike protein of BA.2. The positions of deletions are colored in green, red spheres indicate mutations that lead to enhanced immune escape of BA.2.86, other mutations are shown in blue. For clarity, mutations are only shown in one chain of the spike trimer. (C) Magnified view of one trimer extracted from the model shown in (B) and shown in the same orientation.

Figure 2. BA.2.86 and JN.1 efficiently evade neutralization in double boostered individuals, but the adapted XBB.1.5 vaccine booster enhances protection against both.

(A) Particles pseudo-typed with the indicated S proteins were pre-incubated for one hour at 37 °C with plasma dilutions from double boostered health care workers (biological replicates n=30) (2A) or with plasma dilutions following vaccination with an adapted XBB.1.5 booster (biological replicates n=30) (2B). Pseudo-virus neutralization titer 50 (PVNT50) was calculated using the least squares fit using a variable slope, using a four-parameter nonlinear regression model and values were plotted as geometric mean. Geometric mean standard deviation bars are shown in black. The lower limit of confidence (LLOC) was set at a PVNT50 of 50. Non responders are defined as individuals below 60 (dashed line). All PVNT50 below 10 are set at 10 for visualization purposes. The assay was performed in technical duplicates and with negative controls to assess the virus input of each used pseudo-virus in the absence of plasma antibodies. Percentage of positive responders, geometric means, and fold change neutralization over WT-Wuhan$_{pp}$ are shown on top. Friedman two sided non parametric paired test (ns, $p > 0.05$; *, $p \leq 0.05$; **, $p \leq 0.01$; ***, $p \leq 0.001$). Percentage of positive responders, geometric means, and fold change neutralization over WT-Wuhan$_{pp}$ are shown on top. Source data are provided as a Source Data file.

Figure 3. Mapping mutations in the NTD for effects of BA.2.86 neutralization efficiency in double boostered individuals

(A) Neutralization assessment for particles pseudo-typed with mutations within the NTD of BA.2.86. Each mutant shown contains a single mutation reverting the amino acid mutation in BA.2.86 to the corresponding amino acid within BA.2. Particles pseudo-typed with the indicated S proteins were preincubated for one hour at 37 °C with plasma dilutions from double

boostered health care workers with non-adapted immunogens . The numbers of biological replicates corresponding to individual plasma samples are shown on top. Pseudo-virus neutralization titer 50 (PVNT50) was calculated using the least squares fit using a variable slope, using a four-parameter nonlinear regression model. The lower limit of confidence (LLOC) was set at a PVNT50 of 50. Non responders are defined as individuals below 60 (dashed line) All PVNT50 below 10 are set at 10 for visualization purposes. The assay was performed in technical duplicates and with negative controls to assess the virus input of each used pseudo-virus in the absence of plasma antibodies. Percentage of positive responders, geometric means, and fold change neutralization over WT-Wuhan$_{pp}$ are shown on top. Geometric mean standard deviation bars are shown in black. (B) Individual neutralization data for particles pseudo-typed with mutations within the NTD of BA.2.86. Statistical significance was assessed by Friedman two sided non parametric paired test (ns, $p > 0.05$; *, $p \leq 0.05$; **, $p \leq 0.01$; ***, $p \leq 0.001$). Source data are provided as a Source Data file.

Figure 4. Mapping mutations in the RBD for effects of BA.2.86 neutralization efficiency in double boostered individuals

(A) Neutralization assessment for particles pseudo-typed with mutations within the RBD of BA.2.86. Each mutant shown contains a single mutation reverting the amino acid mutation in BA.2.86 to the corresponding amino acid within BA.2. Particles pseudo-typed with the indicated S proteins were pre-incubated with serum dilutions from immunized health care workers for one hour at 37 °C. The numbers of biological replicates corresponding to individual plasma samples are shown on top. The lower limit of confidence (LLOC) was set at a PVNT50 of 50. Non responders are defined as individuals below 60 (dashed line). Non responders are defined as individuals below this threshold. All PVNT50 below 10 are set at 10 for

visualization purposes. The assay was with negative controls to assess the virus input of each used pseudo-virus in the absence of plasma antibodies. Percentage of positive responders, geometric means, and fold change neutralization over $BA.2_{pp}$ are shown on top. Geometric mean standard deviation bars are shown in black. (B) Individual neutralization data for particles pseudo-typed with mutations within the RBD of BA.2.86. Statistical significance was assessed by Friedman two sided non parametric paired test (ns, $p > 0.05$; *, $p \leq 0.05$; **, $p \leq 0.01$; ***, $p \leq 0.001$). Source data are provided as a Source Data file.

Figure 5. Mapping mutations in the S1/S2 domain for effects of BA.2.86 neutralization efficiency in double boostered individuals

(A) Neutralization assessment for particles pseudo-typed with mutations within the S1/S2 and S2 domain of BA.2.86. Each mutant shown contains a single mutation reverting the amino acid mutation in BA.2.86 to the corresponding amino acid within BA.2. Particles pseudo-typed with the indicated S proteins were preincubated for one hour at 37 °C with plasma dilutions from double boostered health care workers with non-adapted immunogens. The numbers of biological replicates corresponding to individual plasma samples are shown on top. Pseudo-virus neutralization titer 50 (PVNT50) was calculated using the least squares fit using a variable slope, using a four-parameter nonlinear regression model. The lower limit of confidence (LLOC) was set at a PVNT50 of 50. Non responders are defined as individuals below 60 (dashed line). All PVNT50 below 10 are set at 10 for visualization purposes. The assay was performed with negative controls to assess the virus input of each used pseudo-virus in the absence of plasma antibodies. Percentage of positive responders, geometric means, and fold change neutralization over $BA.2_{pp}$ are shown on top. Geometric mean standard deviation bars are shown in black. (B) Individual neutralization data for particles pseudo-typed with mutations

within the S1/S2 and S2 domain of BA.2.86. Statistical significance was assessed by Friedman two sided nonparametric paired test (ns, $p > 0.05$; *, $p \leq 0.05$; **, $p \leq 0.01$; ***, $p \leq 0.001$). Source data are provided as a Source Data file.

Figure 6: Reversions insMPLF16Δ, K460N, K554E and to lesser extent insY144, K484A, and S621P enhance the neutralization efficiency of plasma samples post BNT162b2 XBB.1.5 vaccination.

(A-F) Neutralization assessment for pseudo-typed particles with plasma post BNT162b2 XBB.1.5 vaccination. Each mutant shown contains a single mutation reverting the amino acid mutation in BA.2.86 to the corresponding amino acid within BA.2. Particles pseudo-typed with the indicated S proteins were pre-incubated for one hour at 37 °C with plasma dilutions from double boostered health care workers. Pseudo-virus neutralization titer 50 (PVNT50) was calculated using the least squares fit using a variable slope, using a four-parameter nonlinear regression model. The lower limit of confidence (LLOC) was set at a PVNT50 of 50. Non responders are defined as individuals below this 60 (dashed line). .All PVNT50 below 10 are set at 10 for visualization purposes. The assay was performed in technical duplicates and with negative controls to assess the virus input of each used pseudo-virus in the absence of plasma antibodies. Statistical significance was assessed by Friedman two sided nonparametric paired test (ns, $p > 0.05$; *, $p \leq 0.05$; **, $p \leq 0.01$; ***, $p \leq 0.001$). Source data are provided as a Source Data file.

SARS-CoV2 spike

A)

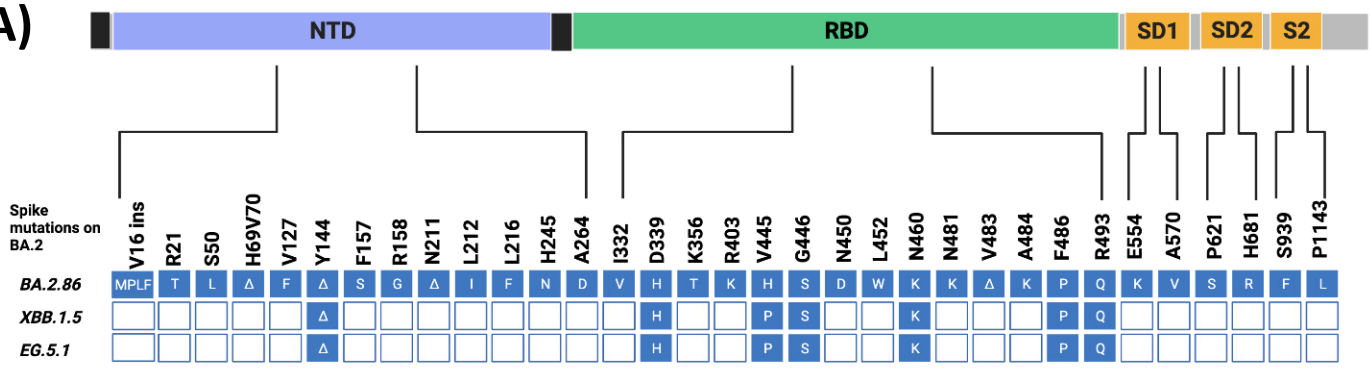

B)

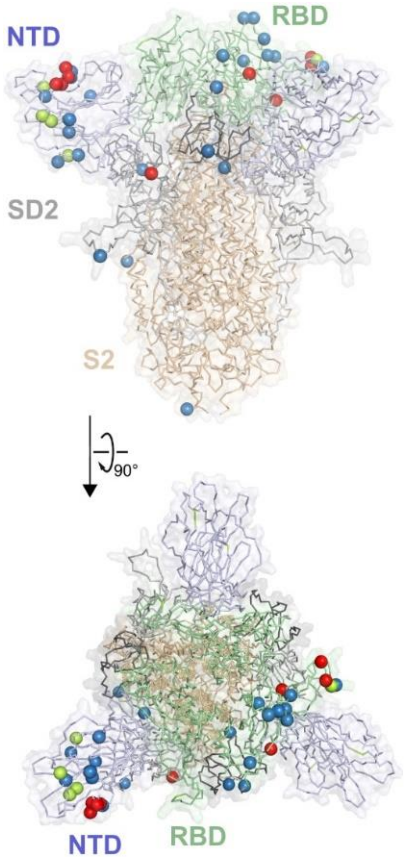

C)

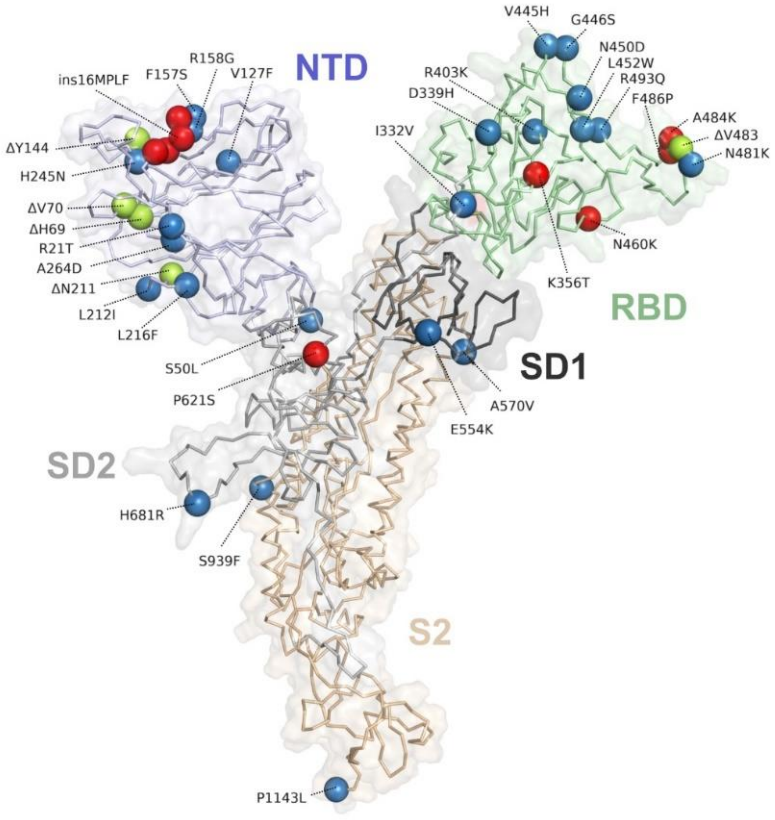

A) **Before XBB.1.5 booster vaccination**

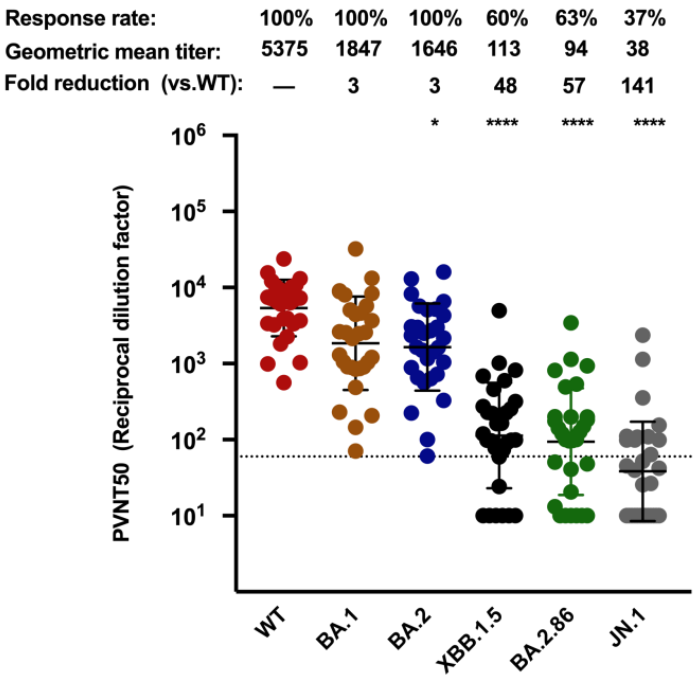

B) **After XBB.1.5 booster vaccination**

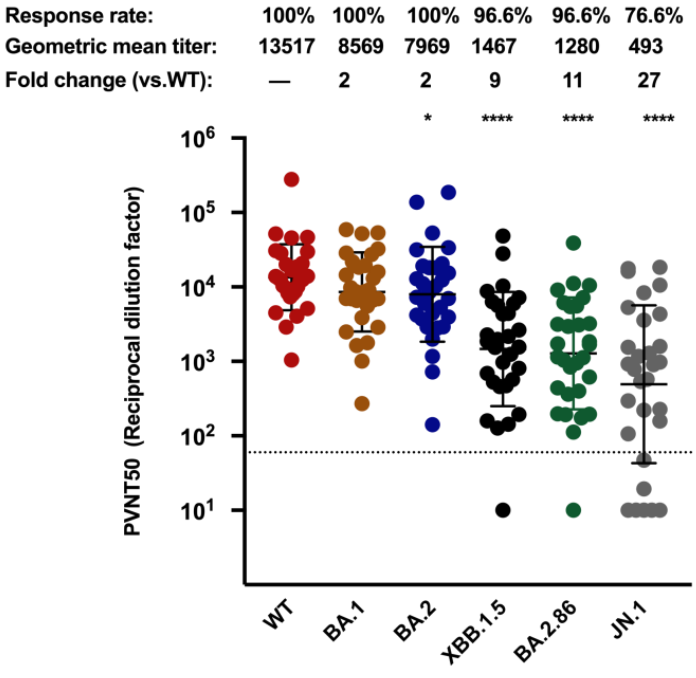

Neutralisation titers for NTD specific BA.2.86pp mutants pre XBB.1.5 adapted vaccine

A)

Geometric mean titer:	1646	94	453	107	60	100	102	85	87	131	112	135	171	122	88
Fold reduction (vs. BA.2):	—	18	4	15	27	16	16	19	19	13	15	12	10	13	19
Sample number:	30	30	21	25	25	18	20	19	19	20	20	21	20	20	23

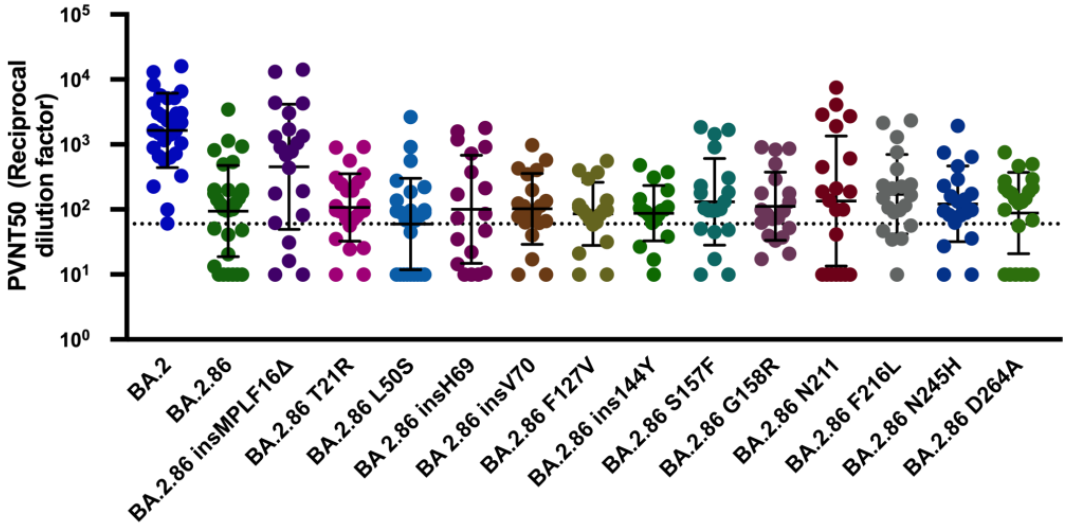

B)

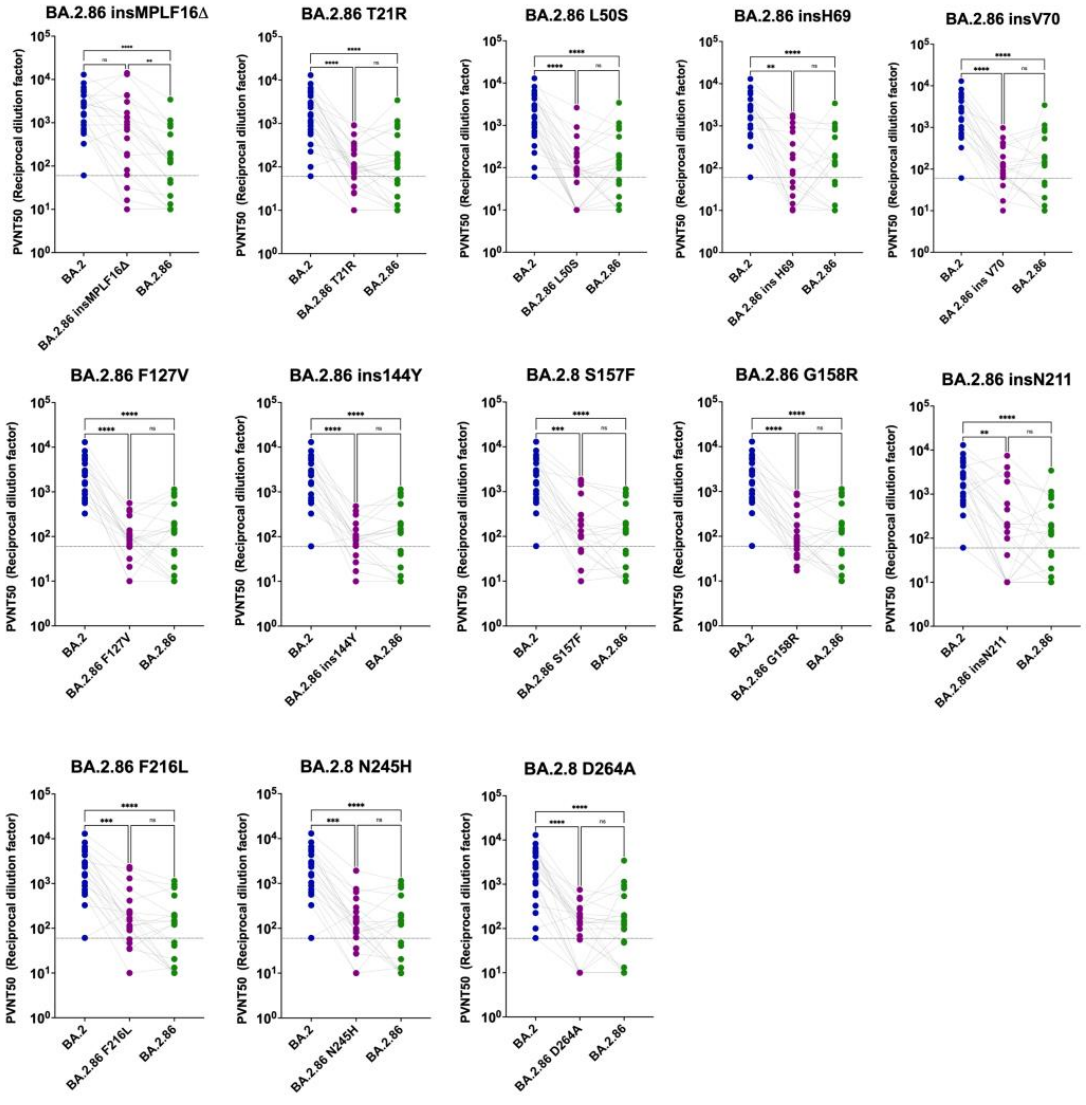

Neutralisation titers for RBD specific BA.2.86pp mutants pre XBB.1.5 adapted vaccine

A)

	BA.2	BA.2.86	BA.2.86 V332I	BA.2.86 H339G	BA.2.86 T356K	BA.2.86 K403R	BA.2.86 H445V	BA.2.86 S446G	BA.2.86 D450N	BA.2.86 W452L	BA.2.86 K460N	BA.2.86 K481N	BA.2.86 Δ483V	BA.2.86 K484A	BA.2.86 P486F	BA.2.86 Q493R
Geometric mean titer:	1646	94	69	100	276	69	92	84	106	95	262	122	242	230	196	51
Fold reduction (vs. BA.2):	-	18	24	16	6	24	18	20	16	17	6	13	7	7	8	32
Sample number:	30	30	25	20	20	20	20	16	20	20	20	21	21	18	18	20

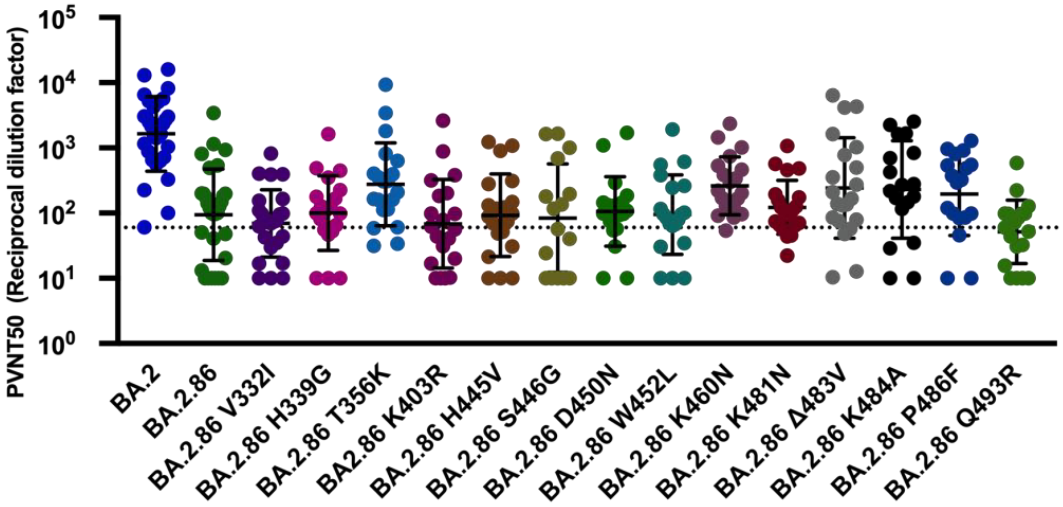

B)

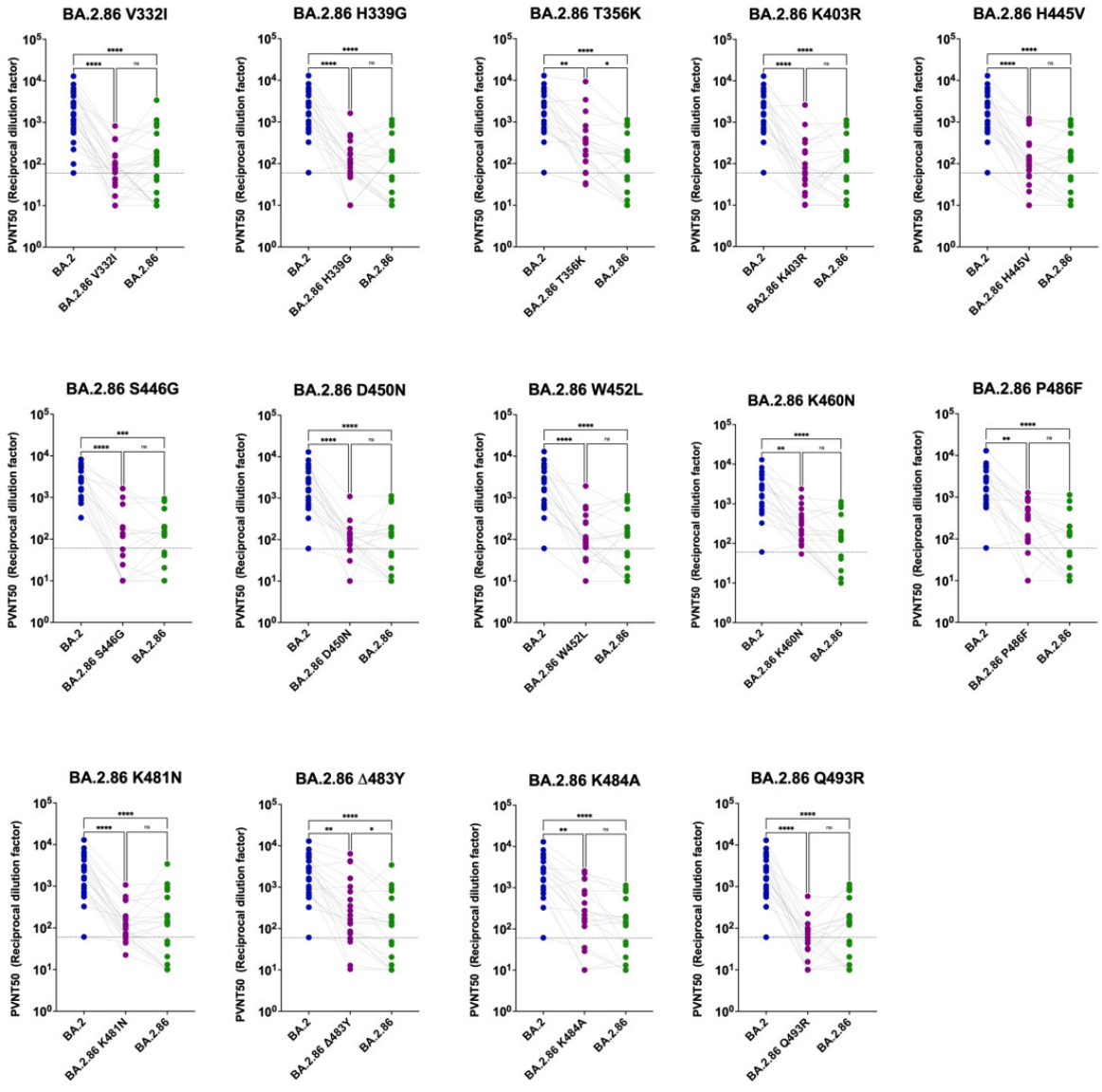

Neutralisation titers for S1/S2 and S2 specific BA.2.86pp mutants pre XBB.1.5 adapted vaccine

A)

	BA.2	BA.2.86	BA.2.86 K554E	BA.2.86 V570A	BA.2.86 S621P	BA.2.86 R681H	BA.2.86 F939S	BA.2.86 L1143P
Geometric mean titer:	1646	94	135	110	437	80	108	68
Fold reduction (vs. BA.2):	—	18	12	15	4	21	15	24
Sample number:	30	30	21	21	20	22	20	20

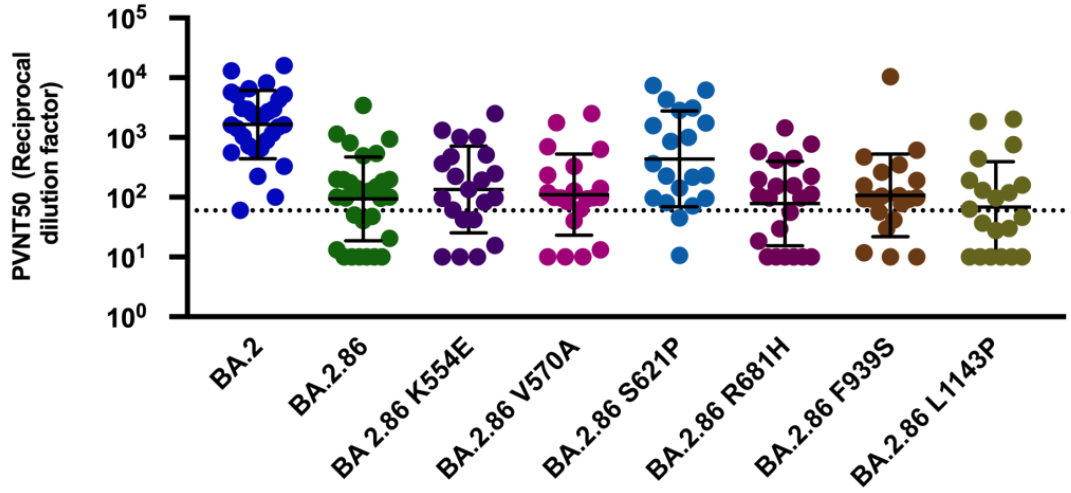

B)

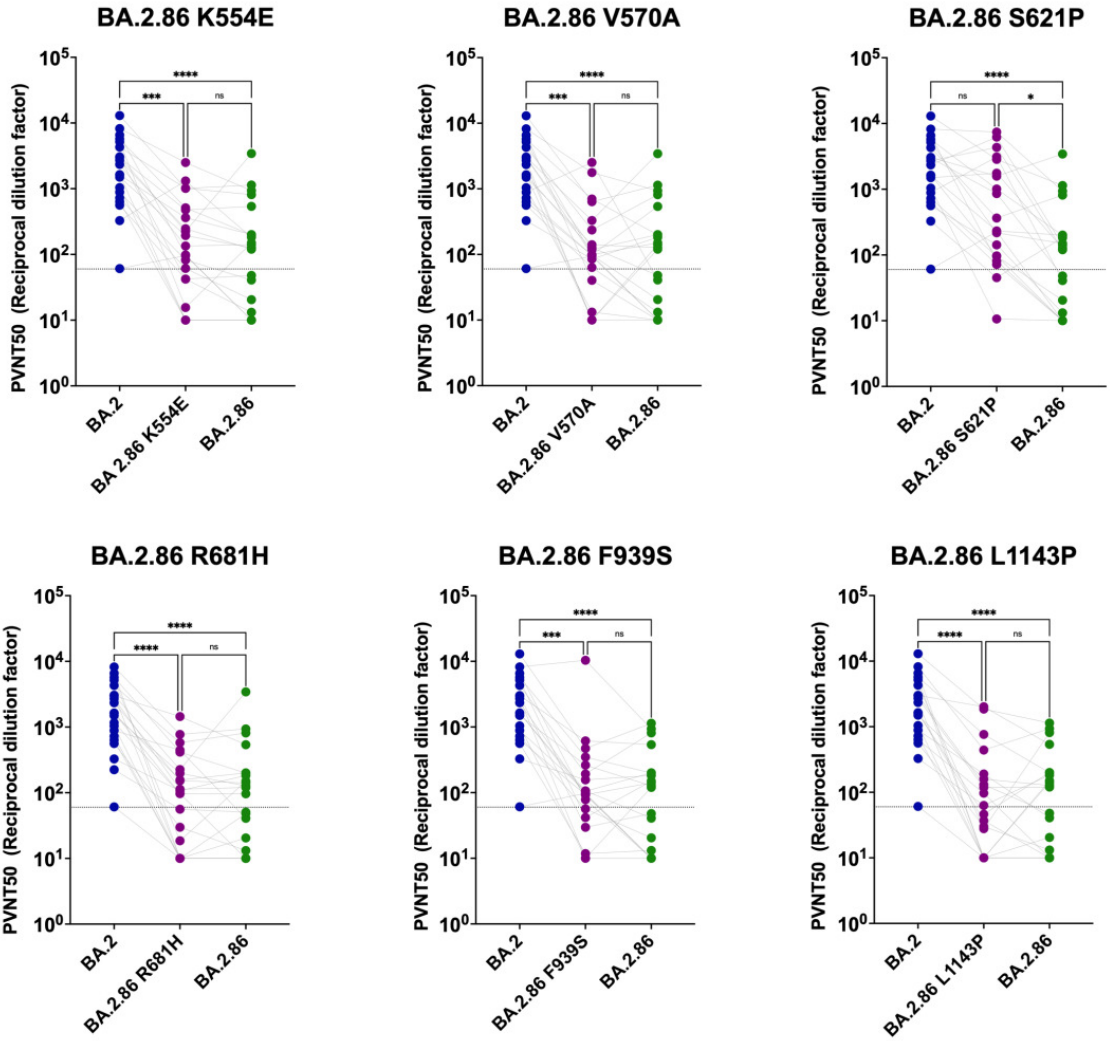

Neutralisation titers for BA.2.86pp mutants post XBB.1.5 adapted vaccine